

Impact of Rituximab Treatment on ^{90}Y -Ibritumomab Dosimetry for Patients with Non-Hodgkin Lymphoma

Sui Shen¹, Andres Forero², Ruby F. Meredith¹, Jatin J. Shah³, Susan J. Knox⁴, Gregory A. Wiseman⁵, Marc E. Usrey², and Albert F. LoBuglio²

¹Department of Radiation Oncology, Comprehensive Cancer Center, University of Alabama at Birmingham, Birmingham, Alabama;

²Department of Medicine, Comprehensive Cancer Center, University of Alabama at Birmingham, Birmingham, Alabama; ³M.D. Anderson Cancer Center, University of Texas, Houston, Texas; ⁴Department of Radiation Oncology, Stanford University Medical Center, Palo Alto, California; and ⁵Division of Nuclear Medicine, Mayo Clinic, Charlton Building I-223, Rochester, Minnesota

To determine whether the therapeutic effect of ^{90}Y -ibritumomab might be enhanced by a full course of rituximab followed by single dose of ^{90}Y -ibritumomab, the trial included pre- and post-rituximab treatment imaging with ^{111}In -ibritumomab and blood pharmacokinetics. Comparison of the pre- and post-rituximab imaging and blood data allowed for the assessment of impact of rituximab on ^{90}Y -ibritumomab dosimetry.

Methods: Seventeen patients with relapsed B cell non-Hodgkin lymphoma first received 250 mg/m² of rituximab plus 185 MBq of ^{111}In -ibritumomab for initial dosimetry evaluation. In weeks 2–4, patients received 3 weekly 375 mg/m² doses of rituximab. In week 6, patients received a 250 mg/m² dose of rituximab plus 185 MBq of ^{111}In -ibritumomab for a second dosimetry evaluation. Five sequential, whole-body γ -camera images were acquired after the ^{111}In -ibritumomab injection. Calculated radiation doses were based on patient-specific organ masses. For each patient, paired comparison of radiation doses before and after rituximab treatment was performed. Paired comparison of residence times for spleen and tumor was also performed.

Results: Before rituximab treatment, the median radiation dose (mGy/MBq) was 0.48 (range, 0.24–0.86) for total body, 3.7 (range, 2.1–11.6) for liver, 6.1 (range, 1.8–17.8) for spleen, 3.3 (range, 2.0–4.7) for kidneys, 2.4 (range, 1.3–3.7) for heart wall, 1.1 (range, 0.4–2.3) for lungs, 0.79 (range, 0.32–1.22) for marrow from blood, and 18.1 (range, 4.7–98.9) for tumor. Paired comparisons were performed in 16 patients only because human anti-murine antibody developed in 1 patient. The median change was 0.007 mGy/MBq for body, –0.14 mGy/MBq for liver, –0.31 mGy/MBq for kidneys, 0.38 mGy/MBq for heart wall, –0.17 mGy/MBq for lungs, and 0.046 mGy/MBq for marrow from blood. The median change in residence time was –0.92 h for spleen and –0.24 h for tumor. The changes were statistically insignificant for total body, liver, kidneys, lungs, and marrow from blood. The median residence times, or mGy/MBq if there were no volume changes, decreased 24% for spleen ($P = 0.0005$) and 28% for tumor ($P = 0.005$). The median radiation dose to heart wall increased 16%, which was statistically significant

($P = 0.002$). **Conclusion:** Changes in ^{90}Y -ibritumomab dosimetry after 4 wk of rituximab treatment were not significant for most organs, except for the heart wall. The reduction of spleen and tumor residence times is more likely to be due to the therapeutic effects of rituximab.

Key Words: monoclonal antibodies; radiobiology/dosimetry; radionuclide therapy; ^{90}Y -ibritumomab; rituximab; Zevalin; dosimetry

J Nucl Med 2010; 51:150–157

DOI: 10.2967/jnumed.109.066597

The non-Hodgkin lymphomas (NHL) are a diverse group of lymphoid neoplasms that collectively rank fifth in cancer incidence and mortality in the United States (1). Chemotherapy treatment with or without radiotherapy can lead to remissions; however, virtually all treated patients with low-grade NHL repeatedly relapse, with shorter remissions after each subsequent course of chemotherapy (2). Additionally, no chemotherapeutic regimen has been shown to be superior to another in prolonging survival in low-grade NHL (3). Ibritumomab is a murine IgG1 κ -monoclonal antibody that is linked to ^{111}In for imaging and ^{90}Y for therapy via the chelator tiuxetan (isothiocyanatobenzyl M–diethylenetriaminepentaacetic acid). Ibritumomab targets the CD20 antigen, which is present on 95% of B-cell lymphomas (4). ^{90}Y -Ibritumomab (Zevalin; BIOGEN/IDEC Pharmaceuticals) yields an overall response rate of 73%, with a response duration of 12 mo when administered as a single nonmyeloablative fraction in relapsed follicular lymphoma (5).

The standard dosing of ^{90}Y -ibritumomab is 11.1 or 14.8 MBq/kg (0.3 or 0.4 mCi/kg, respectively) for platelet count of 100,000–149,000/mm³ or greater than or equal to 150,000/mm³, respectively. The maximal administration dose is 1,184 MBq (32 mCi), regardless of patient body weight (6). The radiolabeled antibody is given after

Received May 26, 2009; revision accepted Oct. 7, 2009.

For correspondence or reprints contact: Sui Shen, Department of Radiation Oncology, University of Alabama at Birmingham, 1824 6th Ave. South, WTI Room 124, Birmingham, AL 35294.

E-mail: sshen@uabmc.edu

COPYRIGHT © 2010 by the Society of Nuclear Medicine, Inc.

250 mg/m² of rituximab (Rituxan; BIOGEN/IDEC Pharmaceuticals). While the dose administration of ⁹⁰Y-ibritumomab is mainly limited by myelotoxicity, unlabeled anti-CD20 mAb, rituximab, does not have a severe myelosuppressive effect (7,8). It was hypothesized that the therapeutic response might be further enhanced by a full course of rituximab, followed by single dose of ⁹⁰Y-ibritumomab, because these 2 treatments do not have spatial additive adverse effects on the same normal organ. However, there was concern that an additional large amount of unlabeled anti-CD20 mAb, rituximab, might adversely alter the pharmacokinetics and dosimetry of ⁹⁰Y-ibritumomab.

To determine whether the therapeutic effect of ⁹⁰Y-ibritumomab might be enhanced by a full course of rituximab, followed by single dose of ⁹⁰Y-ibritumomab, the trial included pre- and post-rituximab treatment imaging with ¹¹¹In-ibritumomab and blood pharmacokinetics. Comparison of paired quantitative imaging and blood data before and after a full course of rituximab treatment allowed for the assessment of changes in ⁹⁰Y-ibritumomab dosimetry as a result of rituximab treatment. To further improve accuracy, dosimetry results were determined using patient-specific organ masses.

MATERIALS AND METHODS

Patients and Study Design

Seventeen patients with histologically confirmed, follicular, or transformed CD20-positive B-cell NHL who had failed at least 1 chemotherapy regimen were enrolled in the present study. No anticancer treatment was allowed for 3 wk before study initiation (6 wk if rituximab, nitrosourea, fludarabine, or mitomycin C), and patients had to have fully recovered from all toxicities associated with prior treatment. Bone marrow involvement with lymphoma was less than 25% from bilateral bone marrow biopsy and aspirate evaluation. Exclusion criteria included prior external radiotherapy to greater than 25% of active bone marrow and the presence of human antimurine antibody (HAMA) reactivity with prior exposure to murine antibodies. Fifteen patients were enrolled at University of Alabama at Birmingham, 1 patient was enrolled at Stanford University, and 1 patient was enrolled at Mayo Clinic. All patients signed written informed consent approved by the corresponding institutional review board. All patients received a first dose of 250 mg of rituximab per square meter, plus 185 MBq (5 mCi) of ¹¹¹In-ibritumomab for the initial dosimetric evaluation. In weeks 2–4, patients received 3 weekly 375 mg/m² doses of rituximab. In week 6, patients received a 250 mg/m² dose of rituximab, plus 185 MBq (5 mCi) of ¹¹¹In-ibritumomab for a second dosimetric evaluation (Fig. 1). Including 1 preload rituximab dose, patients received a total of 1,375 mg of rituximab per square meter in 4 wk before the second ¹¹¹In-ibritumomab dose injection, similar to a full course of rituximab (4 × 375 mg/m²). All patients had measurable lesions assessed with CT at baseline, about 2 wk before the first injection of ¹¹¹In-ibritumomab. CT slices were 3 or 5 mm in thickness. ⁹⁰Y-ibritumomab dosimetry was derived from ¹¹¹In-ibritumomab imaging and paired dosimetric results before and after 3 weekly doses of 375 mg/m².

Rituximab levels were compared in 16 of 17 patients. Paired dosimetric results could not be compared for patient 10 because HAMA developed in the patient after 1,375 mg/m² doses of rituximab in 4 wk. Among the 16 patients, patient 7 had a large body size and weighed 159 kg. Although parts of this patient's arms were outside the γ -camera field of view, all organs were inside the field of view; thus, dose estimates for this patient were not affected.

Rituximab and ¹¹¹In/⁹⁰Y-ibritumomab

Rituximab is a chimeric IgG1 κ -monoclonal antibody. It specifically recognizes the CD20 antigen expressed on normal B cells and most malignant B-cell lymphomas. Rituximab is licensed in the United States as therapy for patients with relapsed or refractory low-grade or follicular, CD20-positive, B-cell NHL. A full course of rituximab consists of 4 weekly doses of 375 mg/m².

Ibritumomab is a murine IgG1 κ -monoclonal antibody that is linked to ¹¹¹In (for imaging) and ⁹⁰Y (for therapy) via the chelator tiuxetan (isothiocyanatobenzyl M-diethylenetriaminepentaacetic acid). ⁹⁰Y-ibritumomab is licensed for the treatment of patients with relapsed or refractory low-grade, follicular, or transformed B-cell NHL, including patients with rituximab-refractory follicular NHL. ⁹⁰Y-ibritumomab is administered in 2 steps: step 1 includes a single 250 mg/m² infusion of rituximab before a fixed dose of 185 MBq (5 mCi; 1.6 mg of antibody). Step 2 follows step 1 by 7–9 d and consists of a second 250 mg/m² infusion of rituximab before 14.8 MBq (0.4 mCi/kg) of ⁹⁰Y-ibritumomab per kilogram.

Quantification of ⁹⁰Y/¹¹¹In in Blood

Whole-blood samples were collected at 30 min and 4, 24, 72, and 144 h after the administration of ¹¹¹In-ibritumomab. ¹¹¹In activity was measured using a γ -well counter, and counts from the sample were converted to activity by co-counting samples with a reference source (9). The reference source containing 19 kBq (0.5 μ Ci) of ¹¹¹In in 1 mL was pipetted from a calibrated stock solution with a known concentration. Activities of ¹¹¹In-ibritumomab were corrected for decay of the radioisotope from the time of drug administration to the time of measurement. ⁹⁰Y-ibritumomab activity in the whole blood was derived from ¹¹¹In activity adjusted by a small difference in physical decay half-life. ⁹⁰Y-ibritumomab concentration was expressed as percentage injected dose per milliliter (%ID/mL) and analyzed using a biexponential clearance (α and β) model. The cumulated activity or residence time was determined with the biexponential clearance parameters (9). Pharmacokinetic results were determined for the first dosimetry study in all 17 patients. Pharmacokinetic results were determined in 15 of 17 patients for the second dosimetry study because HAMA developed in 1 patient after 3 weekly 375 mg/m² doses of rituximab, and blood samples were lost in 1 patient.

Quantitative Imaging

Quantitative imaging for ¹¹¹In has been described previously (9,10). Planar conjugate whole-body images were acquired with a dual-detector γ -camera interfaced to a nuclear medicine computer system. Medium-energy collimators were used to image ¹¹¹In with energy windows centered at 171 and 245 keV (15% width). Transmission scan images were obtained using a ⁵⁷Co sheet source containing about 370 MBq (10 mCi). The same medium-energy collimators were used to image ⁵⁷Co with an energy window centered at 122 keV (15% width). Planar conjugate views of the whole body were acquired immediately

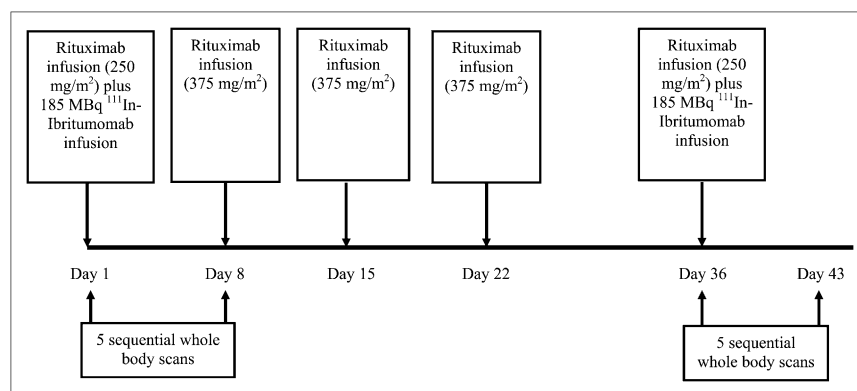


FIGURE 1. Imaging and treatment schematic diagram.

after the administration of ^{111}In -ibritumomab and at 4, 24, 72, and 144–168 h. Whole-body images were acquired in a $256 \times 1,024$ word matrix. Each patient's position on the imaging table and vertical positions of the camera detectors were recorded in the first imaging session and were used throughout the sequential imaging studies for reproducible detector-to-patient positioning (11,12). A 10-mL ^{111}In reference source containing 1.9 MBq (50 μCi) was placed on the imaging table at least 10 cm away from the patient's feet. This calibrated source was used to correct for potential system drift and to convert image region-of-interest (ROI) counts to units of radioactivity adjusted with experimentally measured volume effect.

Before processing images, the operator reviewed ^{111}In -ibritumomab images and CT images with the physician who was familiar with the patient's medical record and CT images for determining organ and tumor ROIs. Major organs that were visible above body background tissue after clearance of the blood pool were contoured, except for the bladder. Although tumors were visible for each patient, tumors were quantified only if they met the following criteria for adequate accuracy: at least 1 g in mass, tumor-to-background pixel count ratio of at least 1.5, and clear tumor ROI boundary. Counts in selected ROIs were corrected for background. The thickness of the background region was equivalent, after accounting for photon attenuation, to the overlapped background tissues in the organ from the anterior and posterior views.

The importance of attenuation correction in quantitative imaging has long been recognized (13,14). We determined activities in the liver and lungs using the geometric-mean quantification.

$$A_{\text{Source}} = \sqrt{I_{\text{Source,anterior}} \times I_{\text{Source,posterior}}} \times \text{ACF} \times f/c, \quad \text{Eq. 1}$$

where $I_{\text{Source,anterior}}$ and $I_{\text{Source,posterior}}$ represent the background-corrected counts per second in the source ROI in anterior and posterior views, respectively. The attenuation-correction factor, ACF, was determined by

$$\text{ACF}_{^{111}\text{In}} = \left(\sqrt{\frac{N_{\text{no pt}}}{N_{\text{pt}}}} \right)^{\frac{\mu_{^{111}\text{In,liver or lungs}}}{\mu_{^{57}\text{Co,liver or lungs}}}}, \quad \text{Eq. 2}$$

where N_{pt} and $N_{\text{no pt}}$ represent the liver or lung ROI counts in the ^{57}Co transmission images with and without the patient, respectively. Equation 2 corrects for the energy differences between ^{57}Co and ^{111}In .

The values for $\mu_{^{57}\text{Co,liver or lungs}}$ and $\mu_{^{111}\text{In,liver or lungs}}$ were determined experimentally using large-volume phantoms (9). The value of f ,

a self-attenuation factor for source thickness, was also experimentally measured instead of calculated using the formula $\mu_s t / \sinh(\mu_s t/2)$ (13,15). c is the camera system calibration factor (counts/s/activity) for that source adjusted with experimentally measured volume effect.

For a source organ that can be clearly visualized only in a single view, previous study suggested that source quantification using a single view is more suitable than using conjugated views (14,16). Kidney, spleen, and tumor activity were quantified using an effective point-source method:

$$A_{\text{Source}} = I_{\text{Source}} \times \exp(\mu_{\text{eff}} \times d)/c, \quad \text{Eq. 3}$$

where I_{Source} is background counts corrected, counts per second in the source ROI of a single-view image. μ_{eff} is the effective linear attenuation coefficient determined using phantoms of 150, 50, and 10 mL. The source depth d is determined from CT images. c is the camera system calibration factor (counts/s/activity) for that source. The depth of kidneys, spleen, and tumors from the body surface were measured from CT images. Phantom sizes and depths were selected to mimic sizes and depths for the liver, spleen, kidneys, and tumors in patients (9). The self-attenuation factor for source thickness is not explicitly included in Equation 2 because our phantom data suggested that the self-attenuation factor was close to 1 for 150- and 50-mL sources.

The uptake of $^{90}\text{Y}/^{111}\text{In}$ in organs and tumors was expressed as percentage of injected dose at various imaging time points. Cumulated activity (and residence time) and biologic clearance half-life were determined by fitting the uptake data with a mono-exponential curve. If fit of a monoexponential curve was not possible as uptake data continuously increased during the period of sequential imaging, cumulated activity was determined using the trapezoid method, and a conservative estimation of the tail was used with a clearance rate of the physical half-life. The cumulated activity or residence time of ^{90}Y was determined from the biodistribution of ^{111}In and adjusted for the small difference in physical half-life between ^{111}In and ^{90}Y .

Organ and Tumor Volumetry Using Patient-Specific Measurements

Baseline CT images before the first injection of 185 MBq (5 mCi) of ^{111}In -ibritumomab were used to determine a patient-specific organ mass to increase the accuracy of the dose estimate. Volume measurements were performed on CT Digital Imaging and Communications in Medicine images using the Eclipse

3-dimensional radiotherapy treatment planning system (Varian Medical System). The tumor, liver, spleen, kidney, and heart volumes were manually defined by individual slice contour drawings on 3- to 5-mm-thick slices. Lung volumes were determined using a contrast-difference edge-detection method, with manual correction for air in the main bronchi. A nominal tissue density of 1 g/cm³ was used for soft tissues, except for the lungs, for which we assumed the lung density to be 0.26 g/cm³ (17). The heart region was defined as extending below the level in which the pulmonary trunk branches into the left and right pulmonary arteries. The activity measured in the heart was assumed to be associated with circulating radiolabeled antibody rather than with uptake in the heart muscle and the mass of the heart wall was calculated.

This retrospective dosimetry analysis was part of a clinical trial to assess the response of the combination of full-course rituximab plus ⁹⁰Y-ibritumomab. Posttreatment CT images were obtained after the completion of all treatments. CT images after the last rituximab dose and before the second dosimetric imaging study were not available. Volumes in the liver, lungs, kidneys, and heart were assumed to be unchanged before and after a full course of rituximab. However, we were not able to assume that the volume of tumors or spleens remained unchanged after a full course of rituximab. It is known that the full course of rituximab, a 4-dose schema approved by the Food and Drug Administration, induced an overall response rate of 48% (18). To assess if spleen volume remained unchanged, the product of the spleen long and short axes (19) in ¹¹¹In-ibritumomab images were measured before and after rituximab treatment.

Radiation Dosimetry with Patient-Specific Organ Mass

Residence times for the liver, spleen, kidneys, lungs, heart, tumor, marrow, and total body were determined from quantitative imaging or counting as described above. The residence time for the remainder of the body was defined as residence time of the total body minus residence times of the liver, spleen, kidneys, lungs, heart, and marrow. These residence times were input into an OLINDA-EXM program for radiation dose calculation (20). The voiding bladder module in the OLINDA-EXM program was used, assuming a voiding interval of 3 h during the day and an interval of 6 h at night (21). The masses of liver, spleen, kidneys, lungs, heart wall, and body of individual patients were used to modify phantom masses in the OLINDA-EXM program. The mass of the individual heart wall was calculated assuming a ratio of 316 to 770 between the heart wall and the heart (wall + content) (22).

To determine ⁹⁰Y concentration in red marrow, the red marrow-to-blood concentration ratio was ascertained with a widely used method described by Sgouros (23). Although the residence time of red marrow for each patient was calculated assuming a reference mass of 1,120 g, the dosimetry result of red marrow from blood was still patient-specific for ⁹⁰Y because the patient-specific marrow dose from β -emissions in the blood does not require an explicit estimate of marrow mass (24).

For the high-energy β -emitter ⁹⁰Y, the absorbed fraction is less than 0.89 for a tumor mass that is less than 20 g (25). Tumor mass and residence time were input into the spheric model module of the OLINDA-EXM program for tumor dose calculation (20).

Statistics

Paired comparisons between tissue radiation dose estimates before and after a full course of rituximab were performed (26).

Normal distribution assumption for the difference before and after was examined by skewness, kurtosis, and omnibus normality tests. If normality could not be rejected by each of these tests, results obtained from a paired *t* test were reported. If normality was rejected, results obtained from a nonparametric test (Wilcoxon signed rank) were reported. Differences in total body, kidneys, lungs, and marrow doses were analyzed with a *t* test. Differences in liver, spleen, heart wall, and tumor were analyzed with the Wilcoxon signed rank test. A comparison was considered statistically significant if the *P* value was less than 0.05.

RESULTS

Organ and Tumor Masses

The median and range for body weights and organ masses are listed in Table 1. Compared with the mass of the reference man's phantom, the observed mass could be 2.2 times higher for the body, 2.5 times lower for liver, 3.8 times higher for spleen, 1.8 times higher for kidneys, 1.9 times lower for lungs, and 2.8 times lower for heart wall (Table 1). Tumor masses ranged from 1 to 282 g (*n* = 28). In those 28 tumors, 9 tumors had masses between 1 and 10 g, 14 tumors had masses between 11 and 50 g, and 5 tumors had masses greater than 50 g.

Impact on ⁹⁰Y-ibritumomab Pharmacokinetics

Blood activities versus time fitted well with a biexponential model. The coefficient of determination (*R*²) for biexponential curve fitting was greater than or equal to 0.99 for all studies (*n* = 32), except for 1 (*R*² = 0.97). Before rituximab treatment, the median peak concentration of ⁹⁰Y-ibritumomab in the whole blood was 0.017 %ID/mL and ranged from 0.012 to 0.035 %ID/mL (*n* = 17). The median β - (slow) effective clearance phase was 31.9 h and ranged from 11.8 to 55.3 h. The median cumulated activity per unit injected dose or area under the curve was 0.0024 h/mL and ranged from 0.0007 to 0.0037 h/mL. The median radiation dose from blood to red marrow was 0.79 mGy/MBq and ranged from 0.32 to 1.22 mGy/MBq.

After 4 wk of rituximab treatment, the median difference in peak concentration of ⁹⁰Y-ibritumomab in whole blood

TABLE 1. Patient Body Weights and Organ Masses Compared with Those of Reference Man (*n* = 17)

Mass (g)	Median	Range	Reference mass in OLINDA
Body	85,280	49,900–159,210	73,700
Liver	1,839	719–2,902	1,910
Spleen	398	112–697	183
Kidneys	372	221–529	299
Lungs	1,255	533–1,709	1,000
Heart	732	351–964	770
Heart wall	300	114–396	316
Tumor (<i>n</i> = 28)	21	1–282	NA

NA = not applicable.

was -0.0015 %ID/mL and ranged from -0.005 to 0.0025 %ID/mL ($n = 15$). The median difference in the β - (slow) effective clearance phase was 1.0 h and ranged from -14.1 to 24.6 h. The median difference in cumulated activity per unit injected dose was 0.0001 h/mL and ranged from -0.0011 to 0.0015 h/mL. The median difference in marrow dose from blood was 0.046 mGy/MBq and ranged from -0.300 to 0.430 mGy/MBq (Fig. 2A). There was no statistically significant difference in red marrow dose before and after rituximab treatment (Table 2).

Impact on ^{90}Y -Ibritumomab Dosimetry

The median radiation dose and range ($n = 17$) for total body, liver, spleen, kidneys, heart wall, lungs, and tumors are listed in Table 2. The paired difference (after rituximab minus before rituximab, $n = 16$) in radiation dose for the total body (Fig. 2B), liver (Fig. 2C), kidneys (Fig. 2E), heart wall (Fig. 2F), and lungs (Fig. 2G) are also listed in Table 2. The median and range for paired difference in residence times were calculated for the spleen (Fig. 2D) and tumor (Fig. 2H) (Table 2).

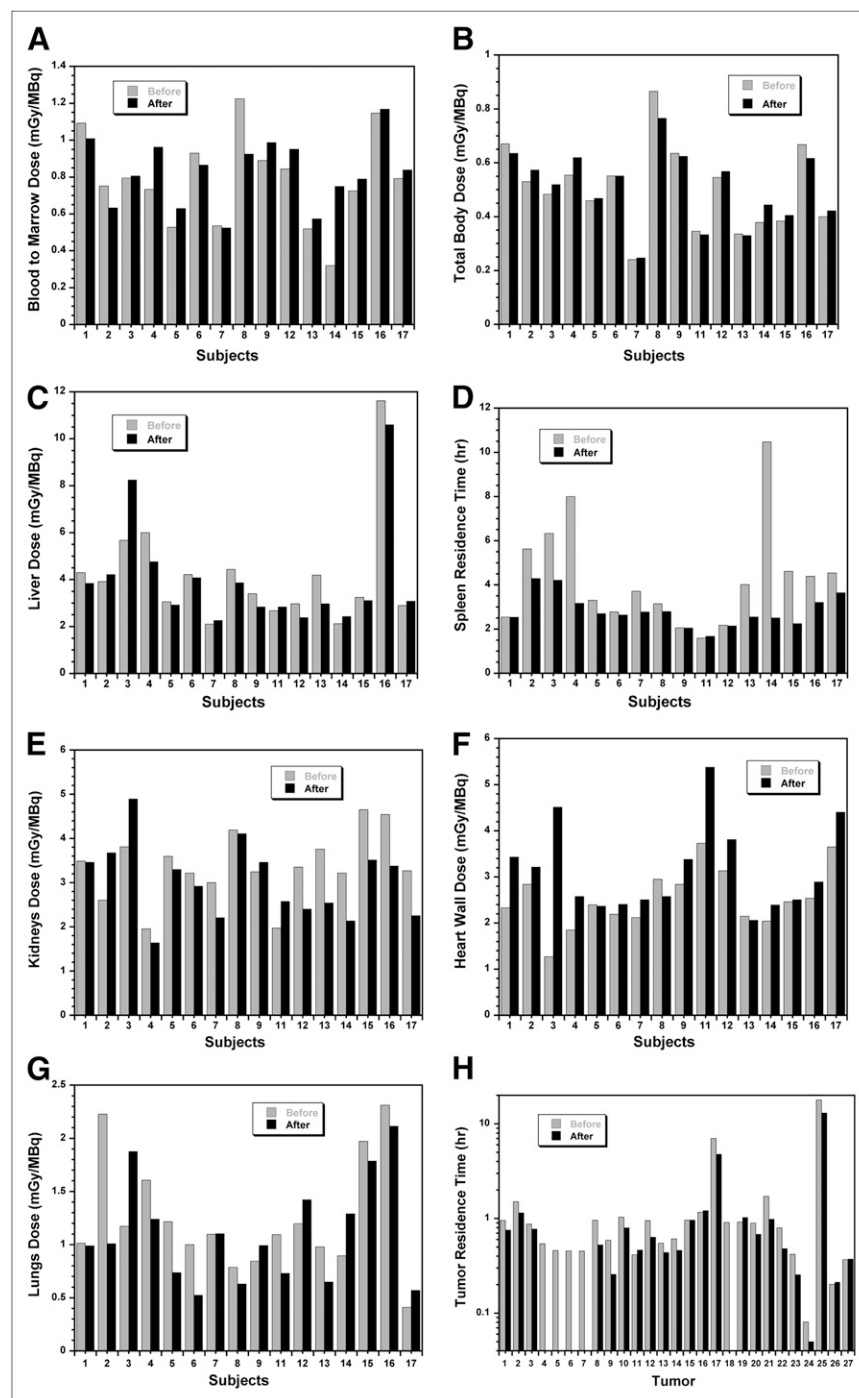


FIGURE 2. Radiation dose to marrow from ^{90}Y -ibritumomab in blood (A), radiation dose to total body (B), radiation dose to liver (C), residence time in spleen (D), radiation dose to kidneys (E), radiation dose to heart wall (F), radiation dose to lungs (G), and residence time in tumor (H). Five of 27 tumors were no longer detectable on γ -camera images at second dosimetry infusion.

TABLE 2. Radiation Dose of ^{90}Y -Ibritumomab (mGy/MBq) Before Rituximab Treatment and Dosimetric Impact of Rituximab Treatment

Tissue	Radiation dose before rituximab treatment ($n = 17$)		Difference in radiation dose before and after rituximab treatment ($n = 16$)		Statistical significance of comparison (significant if $P < 0.05$)
	Median	Range	Median	Range	
Total body	0.48	0.24–0.86	0.007	–0.100–0.065	No ($P = 0.68$)
Liver	3.66	2.11–11.62	–0.14	–1.24–2.55	No ($P = 0.27$)
Spleen*	6.14	1.82–17.76			
Spleen (residence time)	3.86 h	1.59–10.47 h	–0.92 h	–7.96–0.08 h	Yes, decrease ($P = 0.0005$)
Kidneys	3.31	1.95–4.65	–0.31	–1.21–1.08	No ($P = 0.10$)
Heart wall	2.43	1.27–3.73	0.38	–0.37–3.24	Yes, increase ($P = 0.002$)
Lungs	1.10	0.41–2.31	–0.17	–1.22–0.70	No ($P = 0.24$)
Red marrow	0.79	0.32–1.22	0.046 ($n = 15$)	–0.300–0.430	No ($P = 0.37$)
Tumor*	18.1 ($n = 28$)	4.7–98.9			
Tumor (residence time)	0.87 h	0.08–17.9 h	–0.24 h ($n = 27$)	–4.93–0.10 h	Yes, decrease ($P = 0.005$)

*Percentage decrease in dosimetry estimates for spleen and tumor would be identical to percentage decrease in residence time if there were no volume changes after rituximab treatment. However, volume changes were noticed.

There was no significant difference in radiation dose to the total body, liver, kidneys, and lungs before and after rituximab treatment (Table 2). The median radiation dose to the heart wall increased 16% and was statistically significant.

However, the median residence time decreased 24% for the spleen and 28% for tumors after rituximab treatment. These decreases were statistically significant (Table 2). Dosimetry estimates for the tumor or spleen would decrease by the same percentage as that of residence time if there were no volume changes. However, 5 of 27 tumors (excluding 1 tumor of a HAMA patient) were no longer detectable from γ -camera images at the second dosimetry infusion, and posttreatment CT confirmed these tumor responses. For planar image measurements on spleen long and short axis product, 8 of 16 patients (excluding 1 HAMA patient) had a decrease in spleen size greater than 15% at the second dosimetry infusion. The median decrease in spleen size was 14.5%, and the range was 0%–69%.

DISCUSSION

The first ^{131}I -rituximab study for the effect of prior rituximab treatment on subsequent radioimmunotherapy has been recently reported by Illidge et al. (27). For dosimetric evaluation, they assessed changes in the total body dose and marrow radiation dose by examining changes in the effective half-life of the total body and rituximab concentration level in the serum. The current analysis was the first ^{90}Y -ibritumomab dosimetry report for paired comparison in radiation dose change in mGy/MBq for the total body, liver, kidneys, heart wall, lungs, and marrow from blood pharmacokinetics. Radiation dose directly reflects complete information on activity concentration in the tissue over integrated time.

Uptake and clearance can be significantly different when the same monoclonal antibody (Lym-1, CC49, ChL6) is radiolabeled with ^{131}I and ^{111}In (28–36). The difference between ^{131}I -antibody and ^{111}In -antibody was quite prominent in the blood clearance. ^{111}In or another radiometal-labeled antibody generally has faster initial clearance (α -phase), followed by slower secondary clearance (β -phase). This faster initial clearance in the blood is somewhat related to greater liver uptake of the ^{111}In -antibody than the ^{131}I -antibody. Naturally, the impact of rituximab treatment on radiation dosimetry can be different between the $^{111}\text{In}/^{90}\text{Y}$ -rituximab ($^{111}\text{In}/^{90}\text{Y}$ -ibritumomab) reported here and the ^{131}In -rituximab reported by Illidge et al. (27). While Illidge et al. (27) noticed significant increases in radiation dose to total body and marrow based on the increased effective half-life for ^{131}In -rituximab, there was no statistically significant difference in radiation dose to total body and marrow from blood for $^{111}\text{In}/^{90}\text{Y}$ -ibritumomab in the present study. We also observed no statistically significant difference in radiation dose to liver, kidneys, and lungs. However, we did observe a statistically significant decrease in residence time for spleen and tumors, as expected. These decreases were in agreement with the observation made by Illidge et al. (27) for ^{131}In -rituximab. We noticed that an increase in radiation dose to the heart wall was statistically significant ($P = 0.002$), and the median radiation dose increase was 16%. The clinical impact of this increase in the heart wall is unknown, because the heart wall is generally not a dose-limiting factor for $^{111}\text{In}/^{90}\text{Y}$ -ibritumomab.

To further improve dosimetry accuracy, we used patient-specific organ mass for dose calculation. For example, patient 16 had a relatively higher liver dose (Fig. 2C) and a small liver mass of 719 g (Table 1). The error could be substantial if a reference liver mass of 1,910 g was

used. The median organ masses for the liver and heart were close to the reference mass in OLINDA-EXM. The median mass for lungs and kidneys was approximately 25% higher in this group of patients. This group of patients had moderate splenomegaly; the largest spleen mass was 697 g. The organ radiation doses reported here were generally in the same range as previously reported by Cremonesi et al. (37) and Fisher et al. (10) using patient-specific organ masses.

This retrospective dosimetry analysis was part of a clinical trial to assess the response of the combination of full-course rituximab plus ^{90}Y -ibritumomab. The post-treatment CT images were 13 wk after the first dose of ^{111}In -ibritumomab; the tumor or spleen volume at the second ^{111}In -ibritumomab imaging study was unknown. Five of 27 tumors were no longer detectable from γ -camera images at the second dosimetry infusion, and posttreatment CT confirmed these tumor responses. One logical interpretation of this finding is the treatment effect of the rituximab; another possibility could be complete blocking of all CD20 sites in these tumors by rituximab, preventing ^{111}In -ibritumomab binding at the second dosimetry infusion. The median decrease in spleen size (long and short axis product) was 14.5%, and the range was 0%–69% between the two ^{111}In -ibritumomab image sets. While the residence time or cumulated activity per dose injection accurately reflects the change of spleen and tumor in response to rituximab treatment, percentage changes in tumor and spleen dosimetry would be identical to the percentage changes in residence time if there were no volume changes.

CONCLUSION

Changes in ^{90}Y -ibritumomab dosimetry were not significant for most organs after rituximab treatment, except for a 16% increase to the heart wall. The reduction of residence time for spleen and tumor is likely due to therapeutic effects of rituximab on malignant cells in the spleen and tumor.

ACKNOWLEDGMENT

We thank Gayle Hines for her excellent work in patient imaging and sample counting. The clinical trial was supported by BIOGEN/IDEC Inc.

REFERENCES

- Parker SL, Tong T, Bolden S, Wingo PA. Cancer statistics, 1996. *CA Cancer J Clin*. 1996;46:5–27.
- Gallagher CJ, Gregory WM, Jones AE, et al. Follicular lymphoma: prognostic factors for response and survival. *J Clin Oncol*. 1986;4:1470–1480.
- Foon K, Fisher R. Lymphomas. In: Beutler E, Lichtman M, Coller B, et al., eds. *Williams Hematology*. 5th ed. New York, NY: McGraw-Hill, Inc.; 1993.
- Stashenko P, Nadler LM, Hardy R, Schlossman SF. Characterization of a human B lymphocyte-specific antigen. *J Immunol*. 1980;125:1678–1685.
- Gordon LI, Molina A, Witzig T, et al. Durable responses after ibritumomab tiuxetan radioimmunotherapy for CD20+ B-cell lymphoma: long-term follow-up of a phase 1/2 study. *Blood*. 2004;103:4429–4431.
- Zevalin: Full Prescribing Information. Available at: http://www.zevalin.com/pdf/Zevalin_PI_website.pdf. Accessed November 2009.
- Forero A, LoBuglio AF. History of antibody therapy for non-Hodgkin's lymphoma. *Semin Oncol*. 2003;30:1–5.
- Shah J, Wang W, Harrouh VD, et al. Retreatment with yttrium-90 ibritumomab tiuxetan in patients with B-cell non-Hodgkin's lymphoma. *Leuk Lymphoma*. 2007;48:1736–1744.
- Shen S, Forero A, LoBuglio AF, et al. Patient-specific dosimetry of pretargeted radioimmunotherapy using CC49 fusion protein in patients with gastrointestinal malignancies. *J Nucl Med*. 2005;46:642–651.
- Fisher DR, Shen S, Meredith RF. MIRD dose estimate report no. 20: radiation absorbed-dose estimates for ^{111}In - and ^{90}Y -ibritumomab tiuxetan. *J Nucl Med*. 2009;50:644–652.
- DeNardo GL, DeNardo SJ, Macey DJ, Mills SL. Quantitative pharmacokinetics of radiolabeled monoclonal antibodies for imaging and therapy in patients. In: Srivastava SC, ed. *Radiolabeled Monoclonal Antibodies for Imaging and Therapy*. New York, NY: Plenum; 1988:293–310.
- Macey DJ, DeNardo GL, DeNardo SJ. A treatment planning program for radioimmunotherapy. In: Vaeth JM, Meyer JL, eds. *The Present and Future Role of Monoclonal Antibodies in the Management of Cancer: Frontiers of Radiation Therapy and Oncology*. San Francisco, CA: Basel, Karger; 1990:123–131.
- Thomas SR, Maxon HR, Kereiakes JG. In vivo quantitation of lesion radioactivity using external counting methods. *Med Phys*. 1976;3:253–255.
- Siegel JA, Thomas SR, Stubbs JB, et al. MIRD pamphlet no. 16: techniques for quantitative radiopharmaceutical biodistribution data acquisition and analysis for use in human radiation dose estimates. *J Nucl Med*. 1999;40(suppl):37S–61S.
- Hammond ND, Moldofsky PJ, Beardsley MR, Mulhern CB Jr. External imaging techniques for quantitation of distribution of I-131 F(ab')₂ fragments of monoclonal antibody in humans. *Med Phys*. 1984;11:778–783.
- Shen S, DeNardo GL, DeNardo SJ. Quantitative bremsstrahlung imaging of yttrium-90 using a Wiener filter. *Med Phys*. 1994;21:1409–1417.
- International Commission on Radiological Protection (ICRP). *Basic Anatomical and Physiological Data for Use in Radiological Protection: Reference Values*. ICRP publication 23. New York, NY: International Commission on Radiological Protection; 1987.
- McLaughlin P, Grillo-Lopez AJ, Link BK, et al. Rituximab chimeric anti-CD20 monoclonal antibody therapy for relapsed indolent lymphoma: half of patients respond to a four-dose treatment program. *J Clin Oncol*. 1998;16:2825–2833.
- Silverman S, DeNardo GL, Siegel E. Determination of spleen size by scintigraphy. *Cancer Biother Radiopharm*. 1999;14:407–411.
- Stabin MG, Sparks RB, Crowe E. OLINDA/EXM: the second-generation personal computer software for internal dose assessment in nuclear medicine. *J Nucl Med*. 2005;46:1023–1027.
- Thomas SR, Stabin MG, Chen CT, Samarutunga RC. MIRD pamphlet no. 14: a dynamic urinary bladder model for radiation dose calculations. *J Nucl Med*. 1992;33:783–802.
- Stabin MG. MIRDose: personal computer software for internal dose assessment in nuclear medicine. *J Nucl Med*. 1996;37:538–546.
- Sgouros G. Bone marrow dosimetry for radioimmunotherapy: theoretical considerations. *J Nucl Med*. 1993;34:689–694.
- Shen S, DeNardo GL, Sgouros G, O'Donnell RT, DeNardo SJ. Practical determination of patient-specific marrow dose using radioactivity concentration in blood and body. *J Nucl Med*. 1999;40:2102–2106.
- Siegel JA, Stabin MG. Absorbed fractions for electrons and beta particles in spheres of various sizes. *J Nucl Med*. 1994;35:152–156.
- Dawson B, Trapp RG. *Basic & Clinical Biostatistics*. 4th ed. New York, NY: Lange Medical Books/McGraw-Hill; 2004.
- Illidge TM, Bayne M, Brown NS, et al. Phase 1/2 study of fractionated ^{131}I -rituximab in low-grade B-cell lymphoma: the effect of prior rituximab dosing and tumor burden on subsequent radioimmunotherapy. *Blood*. 2009;113:1412–1421.
- DeNardo SJ, DeNardo GL, O'Grady LF, et al. Treatment of B cell malignancies with ^{131}I Lym-1 monoclonal antibodies. *Int J Cancer Suppl*. 1988;3:96–101.
- Meredith RF, Bueschen AJ, Khazaeli MB, et al. Treatment of metastatic prostate carcinoma with radiolabeled antibody CC49. *J Nucl Med*. 1994;35:1017–1022.
- Meredith RF, Khazaeli MB, Plott WE, et al. Phase II study of dual ^{131}I -labeled monoclonal antibody therapy with interferon in patients with metastatic colorectal cancer. *Clin Cancer Res*. 1996;2:1811–1818.
- DeNardo SJ, O'Grady LF, Richman CM, et al. Radioimmunotherapy for advanced breast cancer using I-131-ChL6 antibody. *Anticancer Res*. 1997;17:1745–1751.

32. DeNardo SJ, Richman CM, Goldstein DS, et al. Yttrium-90/indium-111-DOTA-peptide-chimeric L6: pharmacokinetics, dosimetry and initial results in patients with incurable breast cancer. *Anticancer Res.* 1997;17:1735–1744.
33. O'Donnell RT, Shen S, DeNardo SJ, et al. A phase I study of ^{90}Y -2IT-BAD-Lym-1 in patients with non-Hodgkin's lymphoma. *Anticancer Res.* 2000;20:3647–3655.
34. DeNardo GL, O'Donnell RT, Shen S, et al. Radiation dosimetry for ^{90}Y -2IT-BAD-Lym-1 extrapolated from pharmacokinetics using ^{111}In -2IT-BAD-Lym-1 in patients with non-Hodgkin's lymphoma. *J Nucl Med.* 2000;41:952–958.
35. Forero A, Meredith RF, Khazaeli MB, et al. Phase I study of ^{90}Y -CC49 monoclonal antibody therapy in patients with advanced non-small cell lung cancer: effect of chelating agents and paclitaxel co-administration. *Cancer Biother Radiopharm.* 2005;20:467–478.
36. Meredith R, Shen S, Macey D, et al. Comparison of biodistribution, dosimetry, and outcome from clinical trials of radionuclide-CC49 antibody therapy. *Cancer Biother Radiopharm.* 2003;18:393–404.
37. Cremonesi M, Ferrari M, Grana CM, et al. High-dose radioimmunotherapy with ^{90}Y -ibritumomab tiuxetan: comparative dosimetric study for tailored treatment. *J Nucl Med.* 2007;48:1871–1879.



The Journal of
NUCLEAR MEDICINE

Impact of Rituximab Treatment on ^{90}Y -Ibritumomab Dosimetry for Patients with Non-Hodgkin Lymphoma

Sui Shen, Andres Forero, Ruby F. Meredith, Jatin J. Shah, Susan J. Knox, Gregory A. Wiseman, Marc E. Usrey and Albert F. LoBuglio

J Nucl Med. 2010;51:150-157.

Published online: December 15, 2009.

Doi: 10.2967/jnumed.109.066597

This article and updated information are available at:

<http://jnm.snmjournals.org/content/51/1/150>

Information about reproducing figures, tables, or other portions of this article can be found online at:

<http://jnm.snmjournals.org/site/misc/permission.xhtml>

Information about subscriptions to JNM can be found at:

<http://jnm.snmjournals.org/site/subscriptions/online.xhtml>

The Journal of Nuclear Medicine is published monthly.
SNMMI | Society of Nuclear Medicine and Molecular Imaging
1850 Samuel Morse Drive, Reston, VA 20190.
(Print ISSN: 0161-5505, Online ISSN: 2159-662X)

© Copyright 2010 SNMMI; all rights reserved.

 SOCIETY OF
NUCLEAR MEDICINE
AND MOLECULAR IMAGING